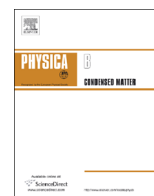




ELSEVIER

Contents lists available at ScienceDirect

Physica B

journal homepage: www.elsevier.com/locate/physb

Refinement of atomic and magnetic structures using neutron diffraction for synthesized bulk and nano-nickel zinc gallate ferrite

S.S. Ata-Allah^{a,*}, A.M. Balagurov^b, A. Hashhash^a, I.A. Bobrikov^b, Sh. Hamdy^a

^a Reactor Physics Department, NRC, Atomic Energy Authority, P.O. Box 13759, Cairo, Egypt

^b Frank Laboratory of Neutron Physics, JINR, 141980 Dubna, Moscow region, Russia

ARTICLE INFO

Article history:

Received 2 July 2015

Received in revised form

10 October 2015

Accepted 26 October 2015

Available online 11 November 2015

Keywords:

X-ray

Mössbauer

HRFD

Zn-Ga-Ni-ferrites

Bulk and nano-scale

Neutron diffraction

Cations distribution

Rietveld method

MRIA and FullProf codes

ABSTRACT

The parent NiFe₂O₄ and Zn/Ga substituted spinel ferrite powders have been prepared by solid state reaction technique. As a typical example, the Ni_{0.7}Zn_{0.3}Fe_{1.5}Ga_{0.5}O₄ sample has been prepared by sol-gel auto combustion method with the nano-scale crystallites size. X-ray and Mössbauer studies were carried out for the prepared samples. Structure and microstructure properties were investigated using the time-of-flight HRFD instrument at the IBR-2 pulsed reactor, at a temperatures range 15–473 K. The Rietveld refinement of the neutron diffraction data revealed that all samples possess cubic symmetry corresponding to the space group Fd3m. Cations distribution show that Ni²⁺ is a complete inverse spinel ion, while Ga³⁺ equally distributed between the two A and B-sublattices. The level of microstrains in bulk samples was estimated as very small while the size of coherently scattered domains is quite large. For nano-structured sample the domain size is around 120 Å.

© 2015 Elsevier B.V. All rights reserved.

1. Introduction

Spinel ferrites have been studied and are considered as well-known materials with “mature” technologies. However, the advances in applications and fabrication technologies in the last 10 years have been impressive. Bulk ferrites remain a key group of magnetic materials, while nano-structured ferrites show a dramatic promise for applications in even significantly wider fields [1–9]. The characteristic physical properties of the spinel ferrites (e.g. electric and magnetic properties) arise from the ability of these compounds to distribute the cations amongst the available tetrahedral A- and octahedral B-sites [10–15].

Spinel with A²⁺B₂³⁺O₄²⁻ formula has a normal cubic spinel structure with oxygen ions forming a cubic close packed lattice with A and B cations occupying the tetrahedral and octahedral coordinated interstices respectively. In the inverse structure, A- and B-cations substitute each other, with the form B[AB]O₄. But in general case, we have (A_δB_{1-δ})[A_{1-δ}B_{1+δ}]O₄, where in parentheses and square brackets cations in A- and B-positions are shown, respectively and the inversion parameter δ can be between 0 and 1 (partially inverted spinel).

Nickel ferrite compound has been investigated by means of

neutron diffraction for the first time about 60 years ago [16]. The inversion parameter for NiFe₂O₄ was δ ≈ 0 and the structural formula can be written as Fe[NiFe]O₄ [17]. In its bulk form, Fe[NiFe]O₄ shows ferrimagnetic order below 850 K. Its magnetic structure consists of two antiferromagnetically coupled sublattices. A first sublattice is formed by ferromagnetically ordered Fe³⁺ (3d⁵, magnetic moment M = 5 μ_B) ions occupying the tetragonal A sites, while the second sublattice contains ferromagnetically ordered Ni²⁺ (3d⁸, M = 2 μ_B) and Fe³⁺ (3d⁵, M = 5 μ_B) ions occupying the octahedral B sites. This type of ordering results in a saturation magnetization of 2 μ_B/f.u. (f.u. = formula unit) [18].

From physical point of view, the cubic-to-tetragonal phase transformation and Jahn–Teller (JT) distortion in the tetragonal phase have attracted considerable attention during many years. In the Reactor and Neutron Physics Department (NRC, Cairo) the substituted spinel compounds are investigated by means of X-ray and Mössbauer techniques to shed more lights on crystallographic structure and the microscopic picture of the magnetic ordering in these diluted ferrimagnets. In particular, the Zn-substituted Cu_{1-x}Zn_xFe_{2-y}Ga_yO₄ compositions were investigated in details [19–22] and it was shown that at x ≥ 0.25, tetragonal-to-cubic transformation occurs.

In continuation of these studies we analyze both the parent compound (NiFe₂O₄) and its two Zn/Ga substituted compositions Ni_{0.7}Zn_{0.3}Fe_{2-y}Ga_yO₄ with y = 1 and 0.5 by means of neutron

* Corresponding author.

diffraction, which is more sensitive to cation distribution than X-rays and Mössbauer to provide more information about atomic and magnetic structure. Additionally to conventionally prepared samples with large crystallite size, a nano-structured composition $\text{Ni}_{0.7}\text{Zn}_{0.3}\text{Fe}_{1.5}\text{Ga}_{0.5}\text{O}_4$ was studied.

2. Experimental details

2.1. Sample preparation

Polycrystalline samples of NiFe_2O_4 , $\text{Ni}_{0.7}\text{Zn}_{0.3}\text{FeGaO}_4$, and $\text{Ni}_{0.7}\text{Zn}_{0.3}\text{Fe}_{1.5}\text{Ga}_{0.5}\text{O}_4$ (referred to as S1, S2 and S3 respectively) are synthesized through solid state reactions using NiO, ZnO, CuO, and Ga_2O_3 as starting materials. The mixture of the oxide powders is pre-fired at 1100 °C for 72 h. The product is reground and fired again at the same conditions to improve homogeneity. Finally, powders are pressed into pellets and sintered at 1200 °C for 8 h, then slowly cooled to room temperature [21,23]. X-ray diffraction (XRD) measurements are obtained and their analysis makes it clear that the products are crystallized in single-phase spinel structure. The $\text{Ni}_{0.7}\text{Zn}_{0.3}\text{Fe}_{1.5}\text{Ga}_{0.5}\text{O}_4$ composition has been prepared again in the nano-scale using sol-gel auto combustion method [24–26], and it is referred to as S4. The $\text{Fe}(\text{NO}_3)_3 \cdot 9\text{H}_2\text{O}$, $\text{Zn}(\text{NO}_3)_2 \cdot 6\text{H}_2\text{O}$, $\text{Ni}(\text{NO}_3)_2 \cdot 6\text{H}_2\text{O}$ and citric acid ($\text{C}_6\text{H}_8\text{O}_7$) were first dissolved in a minimum amount of deionized water to yield a transparent aqueous solution. The mole ratio of citric acid to the total metal cations content was 1:1. The pH value of the solution was adjusted to 7 using ammonia (NH_4OH). The precursor solution was heated at about 80 °C till evaporating all volatile components and water from the beaker and then a very dense gel was formed after which a fluffy dark brown powder was observed at about 200 °C. The fluffy powder was ground mechanically well in agate mortar to produce more fine and dens powder. X-ray diffraction (XRD) measurements are carried out at room temperature using CoK_α radiation. The notation of studied samples, their nominal composition and initially supposed cation distribution are presented in Table 1.

Mössbauer effect (ME) spectra are recorded at room temperature using a time mode spectrometer using a constant acceleration drive with PCAII-1024 channel. The source used is ^{57}Co in Rh matrix with initial activity 50 mCi. Metallic iron spectrum is used for calibration of both observed velocities and hyperfine fields. Absorber thickness is approximately 10 mg/cm² of natural iron. The experimental spectra were fitted by means of a least-squares procedure [27].

2.2. Neutron diffraction measurements

The diffraction patterns were measured with the time-of-flight HRFD instrument at the IBR-2 pulsed reactor in Dubna [28] at several temperatures in the 15–473 K range. At this diffractometer the correlation technique of data acquisition is used, which provides a very high resolution ($\Delta d/d \approx 0.0013$) that is practically

Table 1
Notation, nominal composition and initially supposed cation distribution for the studied samples.

Studied samples		Cations distribution	
Code	Chemical formula	A-site	B-site
S1	NiFe_2O_4	(Fe)	[FeNi]
S3	$\text{Ni}_{0.7}\text{Zn}_{0.3}\text{Ga}_{0.5}\text{Fe}_{1.5}\text{O}_4$	($\text{Fe}_{0.7}\text{Zn}_{0.3}$)	[$\text{Fe}_{0.8}\text{Ni}_{0.7}\text{Ga}_{0.5}$]
S4	$\text{Ni}_{0.7}\text{Zn}_{0.3}\text{Ga}_{0.5}\text{Fe}_{1.5}\text{O}_4$ nano	($\text{Fe}_{0.7}\text{Zn}_{0.3}$)	[$\text{Fe}_{0.8}\text{Ni}_{0.7}\text{Ga}_{0.5}$]
S2	$\text{Ni}_{0.7}\text{Zn}_{0.3}\text{GaFeO}_4$	($\text{Fe}_{0.7}\text{Zn}_{0.3}$)	[$\text{Fe}_{0.3}\text{Ni}_{0.7}\text{Ga}_{0.5}$]

constant in a wide interval of d_{hkl} spacing's. The high-resolution diffraction patterns were collected by several detectors, placed at back scattering angles ($2\theta = \pm 152^\circ$, $d_{hkl} = 0.6\text{--}3.6 \text{ \AA}$) and (90° , $d_{hkl} = 0.8\text{--}4.9 \text{ \AA}$). Additionally, the low-resolution patterns ($\Delta d/d \approx 0.01$) were measured at low scattering angle (PSD at $2\theta = 30^\circ$) for diffraction data collecting up to $d_{hkl} = 16 \text{ \AA}$.

3. Results and discussion

Fig. 1 shows the XRD patterns of the compositions NiFe_2O_4 , $\text{Ni}_{0.7}\text{Zn}_{0.3}\text{FeGaO}_4$, and $\text{Ni}_{0.7}\text{Zn}_{0.3}\text{Fe}_{1.5}\text{Ga}_{0.5}\text{O}_4$ in bulk and nano form respectively. The result of indexing XRD patterns points out that the nominal composition structures with different concentrations are single-phase with no additional lines corresponding to any other phases. The lattice parameters are obtained by fitting the diffraction peaks positions and are found to be only slightly changed with increasing Ga content. This is expected since the radius of Ga^{3+} (0.62 Å) is very close to that of Fe^{3+} (0.64 Å).

Fig. 2 illustrates the ME spectra recorded at room temperature for present compounds. The NiFe_2O_4 (S1) sample shows a well-defined absorption lines fitted with two Zeeman sextets due to Fe^{3+} at the two distinct crystallographic A- and B-sites in the spinel ferrites unit cell. Samples with Ga content show a relaxed spectrum (S3 sample) or even a paramagnetic one (S2 sample). The relaxation effect decreases in the same composition but in nano-scale (S4 sample).

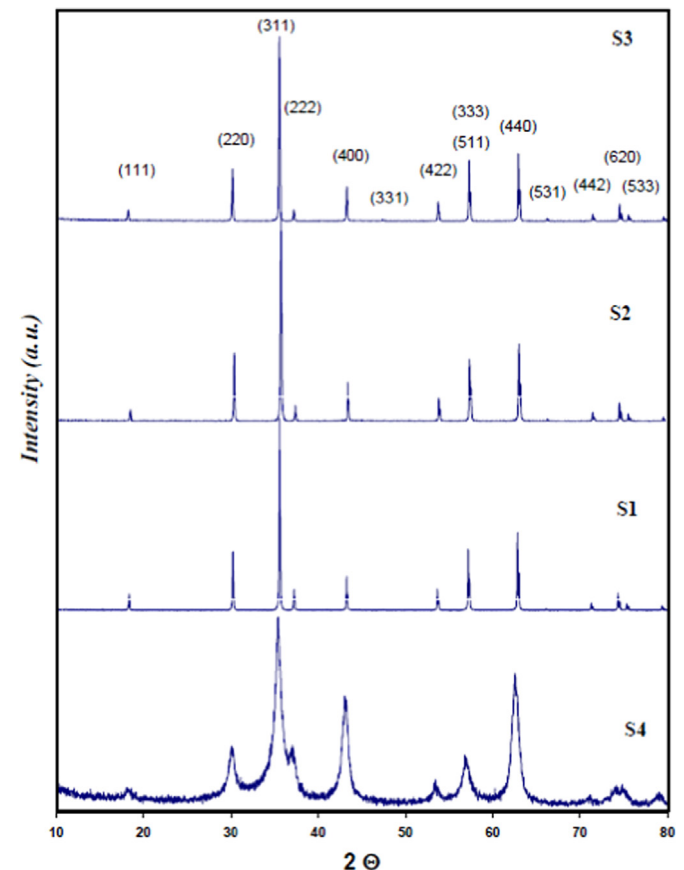


Fig. 1. X-ray diffraction patterns for S1–S4 samples. Miller indices for diffraction lines are shown. The larger widths of diffraction lines of S4 sample are due to “size effect”.

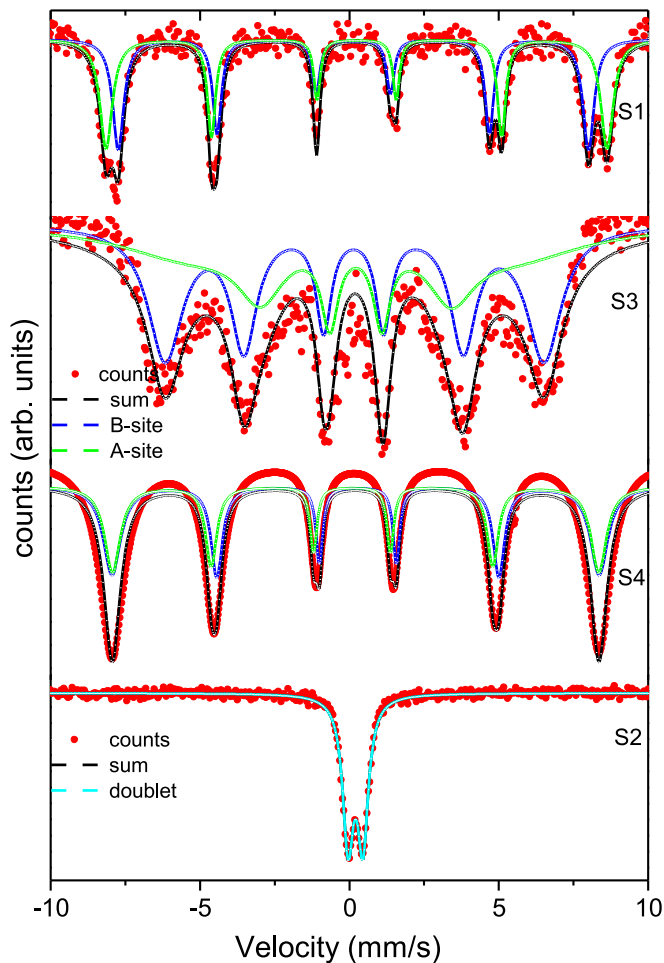


Fig. 2. Mössbauer spectra at room temperature for S1–S4 samples. The S2 sample is in paramagnetic state, others are in ferrimagnetic state with Fe^{3+} at the two distinct crystallographic sites.

3.1. Quadrupole Interaction (2ϵ)

Quadrupole splitting (2ϵ) results from the asymmetrical charge distribution surrounding the Fe ion caused by the electric field gradient (EFG) with varying magnitude, direction, sign and symmetry. In cubic unit cell with Fe^{3+} at A- and B-sites, the Quadrupole splitting (2ϵ) at A-site is due to the asymmetric charge distribution from the 12 B-neighbors. While, at B-site this EFG may arise from departure of the six nearest anion neighbors from their ideal octahedral symmetry and the non-spherical distribution of charges on the next nearest cation and anion neighbors of the B-site. In the present work, Quadrupole splitting (2ϵ) values are negligible (as seen in Table 2). This is due to the overall cubic symmetry of the prepared spinel ferrite and randomness of chemical disorder by which there will be an equal probability for small Quadrupole splitting (2ϵ)'s of opposite signs. Hence, the centers of the Zeeman lines will not change, and consequently

there will be no net observable Quadrupole splitting (2ϵ).

3.2. Isomer shift (δ)

The obtained IS values for the present samples at room temperature are given in Table 2. The obtained result of $\delta(A) < \delta(B)$ in the well-ordered spectra is in agreement with other previously reported data [29–31]. This could be interpreted as being due to the large band separation of $\text{Fe}^{3+}-\text{O}^{2-}$ for the octahedral ions compared with that for the tetrahedral ions. There is no significant change of the IS values with Ga content observed in this spinel system. This means that the s -electron charge distribution of Fe ions is negligibly influenced by gallium substitution.

3.3. Hyperfine fields (H_{hf})

Hyperfine magnetic field H_{hf} at Fe nucleus is proportional to the spontaneous magnetization of the sublattice to which the particular nucleus belongs. H_{hf} measured by ME consists of three contributions: $H_{\text{hf}} = H_{\text{core}} + H_{\text{dip}} + H_{\text{shift}}$, where H_{core} results from polarization of s -electrons by the magnetic moments of d -electrons. This field is larger for free ions than for ions in a crystal because of covalency. H_{dip} represents the dipolar fields produced by the surrounding magnetic ions. This field depends on the distribution of the cation over A- and B-sites. H_{shift} is the supertransferred hyperfine fields at a central cation and originate from the magnetic moments of the nearest neighboring cations, i.e. from the intersublattice contributions h_{AA} and h_{BB} and the intersublattice contributions h_{AB} and h_{BA} . The hyperfine field H_{hf} values for the present compounds at room temperature are given in Table 2. It can be noticed that the hyperfine field H_{hf} decreases as Ga content x increases. This could be explained as; the intersublattice contributions h_{AB} and h_{BA} are predominant in the sample with $x=0.0$. The introduction of Ga^{3+} with closed ($3d^{10}$) shell in place of Fe^{3+} in this unit cell, it replaces Fe^{3+} at the B-site and results in decreasing of these intersublattice contributions and in turns decreases the hyperfine field H_{hf} at both sites.

3.4. Neutron diffraction analysis

The analysis of the diffraction patterns was performed using the Rietveld method by the MRUA [32] and FullProf [33] codes. The refinements were done in the frame of the first setting (without center of symmetry) of the $Fd3m$ (No. 227) space group. In this group the atomic positions for AB_2O_4 spinel with $Z=4$ are: A in (8a) – (0, 0, 0), B in (16d) – (5/8, 5/8, 5/8), O in (32e) with $x=y=z \approx 3/8$. The thermal factors were introduced in isotropic approximation. The next neutron scattering lengths were used in refinements: $b_{\text{Fe}}=0.945$, $b_{\text{Zn}}=0.568$, $b_{\text{Ga}}=0.729$, $b_{\text{Ni}}=1.030$, $b_{\text{O}}=0.581$, all in 10^{-12} cm units.

Firstly, the refinement of the S1 sample was performed, during which the total amounts of Ni and Fe were fixed to 1 and 2, correspondingly, occupancy factors of A- and B-sites were free. At the first stage, the magnetic structure was included in the simplest ferrimagnetic collinear option. The result is shown in Fig. 3, where two peaks with strongest magnetic contribution are indicated. For

Table 2
Mössbauer parameters: hyperfine field (H_{hf}), Quadrupole splitting (2ϵ) and Isomer shift (δ) for the samples in table.

Samples	H_{hfA} (kOe)	H_{hfB} (kOe)	δ_A (mm/s)	δ_B (mm/s)	$2\epsilon_A$ (mm/s)	$2\epsilon_B$ (mm/s)
NiFe_2O_4	489.2 ± 0.09	521.2 ± 0.08	0.1362 ± 0.0016	0.2417 ± 0.0015	0.004 ± 0.006	0.008 ± 0.006
$\text{Ni}_{0.7}\text{Zn}_{0.3}\text{Ga}_{0.5}\text{Fe}_{1.5}\text{O}_4$	342.2 ± 0.14	394.1 ± 0.18	0.1591 ± 0.0018	0.1579 ± 0.0013	-0.115 ± 0.004	0.034 ± 0.006
$\text{Ni}_{0.7}\text{Zn}_{0.3}\text{Ga}_{0.5}\text{Fe}_{1.5}\text{O}_4$ nano	505.8 ± 0.07	506.8 ± 0.08	0.1478 ± 0.0017	0.2450 ± 0.0011	0.122 ± 0.005	-0.076 ± 0.004
$\text{Ni}_{0.7}\text{Zn}_{0.3}\text{GaFeO}_4$	–	–	doublet ^{δ}	–	Q_{doublet}	–
	–	–	0.2044 ± 0.066	–	0.4968 ± 0.056	–

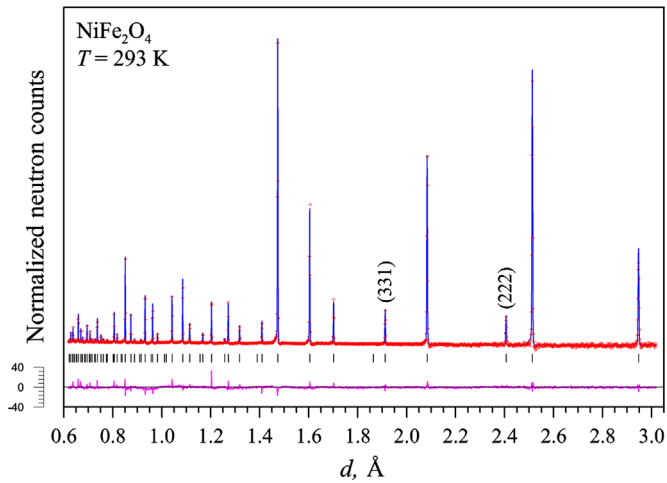


Fig. 3. The diffraction pattern of NiFe_2O_4 powder (the S1 sample) measured at room temperature and processed using the Rietveld method. Vertical ticks indicate the calculated reflection positions. The residual curve is shown at the bottom. Miller indices of the strongest magnetic peaks with practically zero nuclear contribution are indicated.

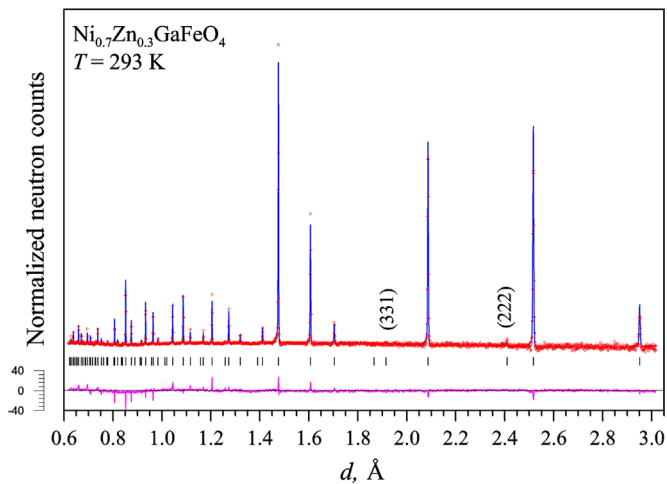


Fig. 4. The same as in Fig. 3 but for $\text{Ni}_{0.7}\text{Zn}_{0.3}\text{GaFeO}_4$ powder (the S2 sample). The magnetic contribution is practically absent.

Table 3

The structural parameters for S1–S4 samples obtained at room temperature; lattice parameter, oxygen position, isotropic thermal factor of cations and oxygen, cation occupancy factors for A- and B-sites, A–O and B–O bond lengths are shown. The conventional experimental (R_e) and weighted (R_w) R-factors (in %) are pointed. Parameters without uncertainties (in brackets) were fixed during refinement. The values of magnetic moments μ are given for A- and B-sites.

Parameter	S1	S2	S3	S4
R_e/R_w	12.0/6.2	15.0/5.9	10.2/8.3	14.3/9.5
a , Å	8.3350 (1)	8.3461 (1)	8.3624 (1)	8.3830 (4)
B_A , Å ²	0.51 (2)	0.87 (8)	1.01 (4)	1.01
B_B , Å ²	0.32 (2)	0.56 (4)	1.01 (4)	1.01
x_O	0.3810 (1)	0.3836 (2)	0.3832 (3)	0.377 (2)
B_O , Å ²	0.80 (2)	0.88 (5)	1.30 (7)	1.30
n_{Fe} , A/B-sites	0.99/1.01 (1)	0.23/0.77 (2)	0.42/1.08 (2)	0.42/1.08
n_{Ni} , A/B-sites	0.01/0.99 (1)	0/0.7	0/0.7	0/0.7
n_{Zn} , A/B-sites	–	0.3/0	0.3/0	0.3/0
n_{Ga} , A/B-sites	–	0.47/0.53 (2)	0.28/0.22 (2)	0.28/0.22
A–O, Å	1.891 (1)	1.931 (1)	1.929 (1)	1.84 (1)
B–O, Å	2.035 (1)	2.017 (1)	2.024 (1)	2.08 (1)
μ (A/B-sites), μ_B	4.5 (2)/3.1 (2)	–	0.93(13)/2.03(6)	–
L , Å	3300(100)	1660 (50)	1530 (50)	120 (10)

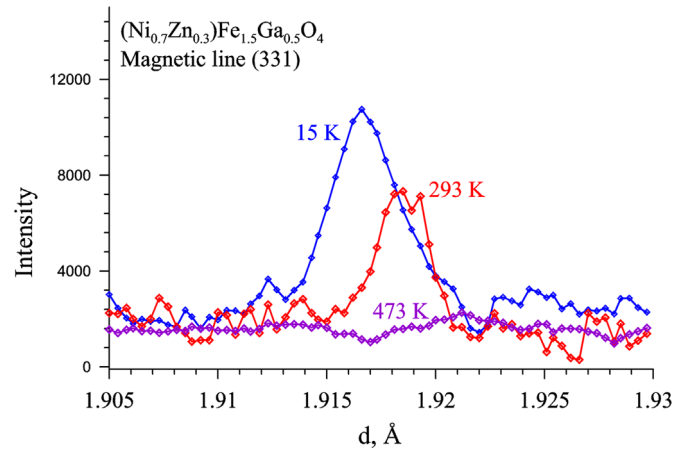


Fig. 5. Diffraction peak (331) of the S3 sample measured at low, room and high temperatures. Nuclear structure factor for this peak is close to zero. Magnetic contribution is absent after 200 °C.

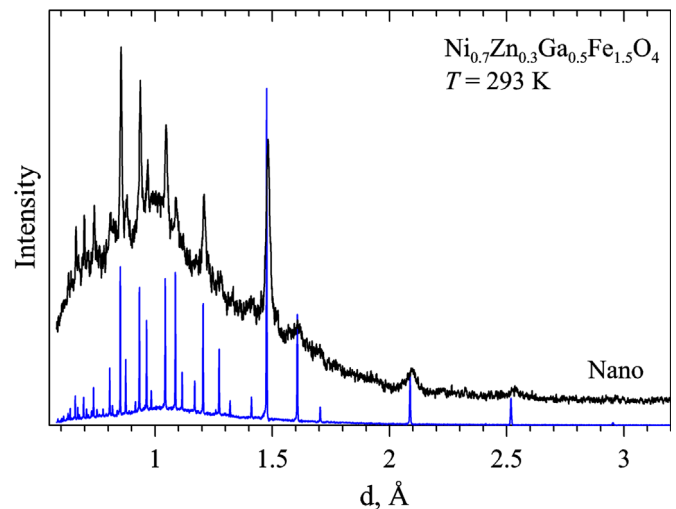


Fig. 6. Comparison of diffraction patterns measured with S3 and S4 (nano-structured) samples. The diffraction lines of the S4 sample are about 15 times wider than of the S2 one. Positions of diffraction peaks are close in both samples.

occupancy factors of A- and B-sites we obtain: $n(A)=1.010(4)$, $n(B)=1.990(4)$. It means that this spinel has the structural formula as $(\text{Fe})[\text{NiFe}]\text{O}_4$ with precision of about 1% that perfectly matches literature data [17]. Correlation with thermal factors, which often complicates the determination of the occupancies, in our case is not expressed strongly due to the very large d_{hkl} -range and the presence of a large number of well-resolved diffraction peaks. The important result of this analysis is the confirmation of a possibility to find occupancy factors with good accuracy despite the contrast between Fe and Ni is not high.

For refinement of the S2 and S3 samples, as a starting point, we suppose that all Ni atoms are in B-sites, Fe is substituted for Zn in the A-site and all Ga atoms are in B-site. For this the coherent scattering lengths for A and B sites are: $b_A=0.832$, $b_B=0.867$ for S2 and $b_A=0.832$, $b_B=0.921$ for S3 again in 10^{-12} cm units. Refinements of all measured patterns (an example is presented in Fig. 4) show that n_A is systematically smaller than 1 and, contrary, n_B is systematically higher than 2. The only hypothesis, which is compatible with these changes, is interchange of Fe in A-site and Ga in B-site because $b_{\text{Ga}}=0.729 < b_{\text{Fe}}=0.945$. Thus we have two equations (for n_A and n_B occupancies) for one unknown quantity (content of Ga in A-site). After averaging we obtain that in S2 and S3 samples $n_A(\text{Ga})=0.28(2)$ and $0.47(2)$ respectively, which means

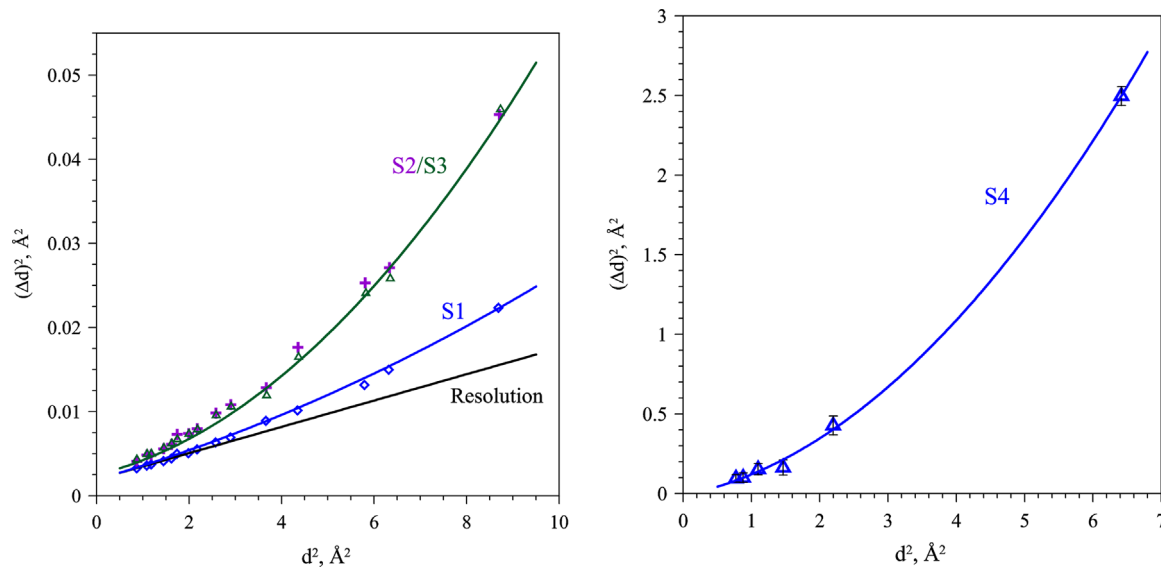


Fig. 7. Dependence of widths of diffraction lines on d -spacing for S1–S3 samples (on the left) and S4 (on the right). Experimental points and approximation curves are shown. The points for S2 (crosses) and S3 (triangles) are practically coincide (for clarity, only one curve is shown). The statistical errors for S1–S3 experimental points are close to the sign size. The contribution of the HRFD resolution function, measured with a standard sample, is also shown. The $(\Delta d)^2$ values are multiplied by 10^3 .

that the real compositions of these samples are:

S2: $(\text{Fe}_{0.23}\text{Ga}_{0.47}\text{Zn}_{0.3}) \cdot [\text{Fe}_{0.77}\text{Ni}_{0.7}\text{Ga}_{0.53}]\text{O}_4$, S3: $(\text{Fe}_{0.42}\text{Ga}_{0.28}\text{Zn}_{0.3}) \cdot [\text{Fe}_{1.08}\text{Ni}_{0.7}\text{Ga}_{0.22}]\text{O}_4$.

Thus, we may conclude that in both samples around 50% of Ga atoms are shifted in the A-site. The structural parameters for all samples and results of calculations of Ga content are shown in Table 3. Thermal parameters of A- and B-cations of samples S2 and S3 are considerably higher than for the parent compound, which is probably due to the larger fluctuations of ionic radii. Moreover, for the sample S3 to stabilize the refinement process we had to use the constrain $B_A=B_B$.

The S1 and S3 samples are ferrimagnetic with $T_C \approx 850$ K and 420 K, correspondingly. The magnetic contribution in the intensities of diffraction peaks is clearly seen (Fig. 5). Despite the magnetic structure is not a subject of this paper, the preliminary refinement of the values of magnetic moments was performed. For this the FullProf package was used, with the magnetic form factor of Fe^{3+} for both A- and B-sites. The obtained data are presented in Table 3.

3.5. Analysis of sample microstructure

The very high resolution of the HRFD instrument provides an opportunity for analysis of microstructural characteristics of studied samples, namely, the level of microstrains and the average size of coherently scattered domains. The comparison of diffraction patterns measured with S3 and S4 (nano-structured) samples is presented in Fig. 6. One can see their common identity, and a notable increase in the level of the incoherent background arising from the noncrystalline fraction in addition to peak broadening (more than 10 times).

For estimation of the microstructural characteristics the following relation can be used [34]:

$$W(d)^2 = C_1 + (C_2 + C_3)d^2 + C_4d^4,$$

where W is the width of diffraction lines (FWHM or integral one), measured for a set of d_{hkl} , C_1 and C_2 are known values, described the resolution function of HRFD, C_3 and C_4 are connected with microstrains in a sample and size of coherently scattered blocks, correspondingly. As it is known $C_3 \approx (2\epsilon)^2$ and $C_4 \approx (k/L)^2$, where k depends on the shape of the blocks and usually is close to 1. The obtained $W(d)^2$ dependences for all S1–S4 samples are

shown in Fig. 7. The level of microstrains is very low for all samples and can not be estimated adequately. The size effect is quite definite and can be estimated as $L \approx 3300$ Å for S1 and as $L \approx 1600$ Å for both S2 and S3. The smaller number of intensive peaks in the nano-structured sample prevents the same precision in size determination. Moreover, it depends on d -spacing range, which is used for calculations and can be estimated roughly as $L \sim 120$ Å. The obtained microstructural information is included in Table 3.

4. Conclusions

Single-phase cubic spinel ferrites NiFe_2O_4 and $\text{Ni}_{0.7}\text{Zn}_{0.3}\text{Fe}_{2-y}\text{Ga}_y\text{O}_4$ with $y=1$ and 0.5 in the bulk and nano-structured forms were synthesized. Refinement of atomic structure through precise analysis of neutron diffraction patterns measured with high-resolution TOF-diffractometer was done. Obtained results confirm that at room temperature the NiFe_2O_4 parent compound is a fully inverted spinel ($\delta=0 \pm 0.01$) with the cubic symmetry of the lattice. The analysis of Zn/Ga doped compositions shows that the cubic symmetry is preserved; all Zn ions are in A-sites, while Ga ions are distributed equally between A- and B-sites of spinel structure. No structural or magnetic phase transitions were found down to 10 K. The level of microstrains was estimated as very small while the size of coherently scattered domains is quite large.

Acknowledgments

The authors are grateful to V.G. Simkin for substantial help in carrying out the experiments at the HRFD. The work was performed with the financial support from the Russian Scientific Foundation (Project no. 14-12-00896).

References

- [1] A. Verma, M.I. Alam, R. Chatterjee, T.C. Goel, R.G. Mendiratta, J. Magn. Mater. 300 (2006) 500.
- [2] V. Zaspalis, V. Tsakaloudi, E. Papazoglou, M. Kolenbrander, R. Guenther, P.V. D. Valk, J. Electroceram. 13 (2004) 585.

- [3] E.J. Brandon, E.E. Wesseling, V. Chang, W.B. Kuhn, *IEEE Trans. Compon. Packag. Technol.* 26 (2003) 51.
- [4] M. Angeli, E. Cardelli, E. Della Torre, *Physica B* 275 (2000) 154.
- [5] P.R. Wilson, J.N. Ross, A.D. Brown, *IEEE Trans. Magn.* 40 (2004) 1537.
- [6] G. Stojanovic, M. Damnjanovic, V. Desnica, et al., *J. Magn. Magn. Mater.* 297 (2006) 76.
- [7] Z.W. Li, L. Guoqing, L. Chen, W. Yuping, C.K. Ong, *J. Appl. Phys.* 99 (2006) 063905.
- [8] B.W. Li, Y. Shen, Z.X. Yue, W.C. Nan, *Appl. Phys. Lett.* 89 (13) (2006) 132504.
- [9] R.C. Che, C.Y. Zhi, C.Y. Liang, X.G. Zhou, *Appl. Phys. Lett.* 88 (2006) 1.
- [10] S.S. Ata-Allah, *J. Magn. Magn. Mater.* 284 (2004) 227.
- [11] S.S. Ata-Allah, M. Kaiser, *Solid Status Solidi A* 201 (14) (2004) 3157.
- [12] S.S. Ata-Allah, F.M. Sayedahmed, M. Kaiser, A.M. Hashhash, *J. Mater. Sci.* 40 (2005) 1–8.
- [13] M. Kaiser, S.S. Ata-Allah, *Mater. Res. Bull.* 44 (2009) 1249.
- [14] S.S. Ata-Allah, M. Yehia, *Phys. B Condens. Matter* 404 (2009) 2382.
- [15] A. Hashhash, M. Yehia, S.M. Ismail, S.S. Ata-Allah, *J. Supercond. Nov. Magn.* 27 (10) (2014) 2305.
- [16] J.M. Hastings, L.M. Corliss, *Rev. Mod. Phys.* 25 (1953) 114.
- [17] D. Carta, et al., *J. Phys. Chem. C* 113 (2009) 8606.
- [18] U. Luders, et al., *Phys. Rev. B* 71 (2005) 134419.
- [19] S.S. Ata-Allah, *J. Solid State Chem.* 177 (2004) 4443.
- [20] S.S. Ata-Allah, M. Yehia, *Physica B* 404 (2009) 2382–2388.
- [21] M.K. Fayek, S.S. Ata-Allah, H.A. Zayed, M. Kaiser, S.M. Ismail, *J. Alloy. Compd.* 469 (2009) 9.
- [22] S.S. Ata-Allah, A. Hashhash, *J. Magn. Magn. Mater.* 307 (2006) 191–197.
- [23] Abdul Samee Fawzi, A.D. Sheikh, V.L. Mathe, *J. Alloy. Compd.* 502 (2010) 231.
- [24] S.A. Seyyed Ebrahimi, S.M. Masoudpanah, *J. Magn. Magn. Mater.* 357 (2014) 77.
- [25] P. Priyadharsinia, A. Pradeepa, P. Sambasiva Raob, G. Chandrasekarana, *Mater. Chem. Phys.* 116 (2009) 207.
- [26] M.A. Gabal, W.A. Bayoumy, *Polyhedron* 29 (2010) 2569.
- [27] G. Grosse, *Mos-90, Version 2.2, 2nd ed.*, (Oskar-Maria-Graf-Ring, München), 1992.
- [28] A.M. Balagurov, *Neutron News* 16 (2005) 8.
- [29] E. Sionanek, Z. Sroubek, *Phys. Rev.* 163 (1960) 275.
- [30] D.C. Khan, M. Misra, A.R. Das, *Phys. Rev.* 53 (1982) 2722.
- [31] R.V. Pound, G.A. Rebka, *Phys. Rev. Lett.* 4 (1960) 274.
- [32] V.B. Zlokazov, V.V. Chernyshev, *J. Appl. Cryst.* 25 (1992) 447.
- [33] J. Rodriguez-Carvajal, *Physica B* 192 (1993) 55.
- [34] V.L. Aksenov, A.M. Balagurov, V.A. Trounov, *J. Neutron Res.* 6 (1997) 135.